Available online at www.sciencedirect.com

SCIENCE DIRECT®

PERGAMON

International Journal of Multiphase Flow 29 (2003) 959–982

International Journal of Multiphase Flow

www.elsevier.com/locate/ijmulflow

The effect of particle interactions on the sedimentation process of non-cohesive particles

Zu-Jia Xu *, Efstathios E. Michaelides

School of Engineering and Center for Bioenvironmental Research, Tulane University, New Orleans, LA 70118, USA

Received 20 September 2002; received in revised form 30 March 2003

Abstract

The sedimentation process of solid particles in a two-dimensional channel with an initially homogeneous, square configuration is numerically investigated at Reynolds numbers up to 10. The Lattice Boltzmann method is used to simulate the hydrodynamic interactions between fluid and particles. During the process the dispersion of particles in the horizontal direction fluctuates around zero, while the dispersion in the vertical direction (along the gravity direction) increases almost linearly. The increasing rate heavily depends on the initial symmetry of the suspension. The simulations show that the process of sedimentation encompasses three stages. In the first stage, the initial particle configuration plays a major role on the average velocity of the particles. A V-shape or W-shape front may be formed by the particles. During the second stage, the concentration is lower, strong particles interactions occur and the formation and destruction of particle clusters play a major role in the process. The sedimentation velocity depends to a large extent on the number of clusters formed and the velocity field developed. During the third stage, the concentration becomes low and the particle clusters are stable. The wakes generated by particle and clusters, especially of the leading cluster becomes important in the process. Average and fluctuation velocity have been obtained in the simulations and are reported in this paper.

Keywords: Sedimentation; Particles; Lattice Boltzmann; Hydrodynamic force; Clusters

1. Introduction

Sedimentation of particles is one of the most important phenomena in suspension flows with a multitude of practical applications ranging from environmental sediment precipitation to

* Corresponding author. Tel.: +1-504-865-5061.
E-mail address: zxu@tulane.edu (Z.-J. Xu).

0301-9322/03/$ - see front matter
doi:10.1016/S0301-9322(03)00060-0

industrial separation processes. A key to the sedimentation problem is the determination of the hydrodynamic force between groups of particles and the viscous fluid. While the hydrodynamic force on a single particle translating in a viscous fluid has been well studied, starting with the work of Stokes (1845), the motion of groups of particles is more complicated and not well understood. Among the most successful approaches used for the behavior of groups of particles are average methods, such as the method by Segrè et al. (2001) who introduced the concept of "effective temperature" to describe the random behavior in the velocities of the particles that constitute the suspension.

Richardson and Zaki (1954) derived an empirical formula for the sedimentation velocity of a suspension as a function of its concentration. Batchelor (1972) derived analytically that at very low concentrations ($\phi \ll 1$) the average particle velocity depends linearly on the concentration of the particles, that is $V = V_t \cdot (1 - n\phi)$, which may be considered as the first-order expansion of Eq. (1). Davis and Acrivos (1985) found experimental evidence for this relationship at low concentration ($\phi < 5\%$). DiFelice (1999) conducted experiments within a wide range of Reynolds number ($0.001 < Re < 1000$) and verified the linear dependence of the velocity on the concentration for dilute suspensions at $\phi < 5\%$. Nicolai et al. (1995) carried out an experimental study on the velocity fluctuations at volume concentration up to 40% and concluded that Richardson–Zaki formula fits fairly well their results. Caflisch and Luke (1985) considered the particle velocity fluctuation based on the analysis by Batchelor (1972) and pointed out that the variance of particle velocities depends on the container size: the larger the container, the higher the velocity fluctuations. Ladd (1997) proved numerically this conclusion by using the Lattice-Boltzmann method (LBM) to calculate the statistics of 32,000 particles settling under gravity. He observed that the velocity fluctuations in both vertical and horizontal directions change linearly with respect to the width of the box at $\phi = 0.1$. However, this may be an open question since the experimental results by Nicolai and Guazelli (1995) as well as Segrè et al. (1997) indicate that, at least in the range $0.01 < \phi < 0.05$, the velocity fluctuations are independent of the size of the settling chamber. More recently, Agrawal et al. (2001) used a continuum model to investigate clusters in dilute gas-particle flows ($\phi < 0.1$). Their simulations showed that the meso-scale structures affect the interaction force that couples the gas the particle phases. They also increase the viscosity of the two phases and the normal stresses in the particle phase. Bunner and Tryggvason (2002) studied the properties of the fluctuation velocity of the bubbles and the liquid-phase turbulence in homogeneous bubbly flows for a system of 216 sphere bubbles and Reynolds numbers up to 30.

Regarding the methods of modeling of a suspension of particles, Brady and Bossis (1985) employed the Stokesian dynamics model to simulate the flow of a group of particles under the creeping flow condition ($Re \approx 0$). In this case, the inertia of both the fluid and particles is neglected. Recently, Climent and Maxey (2001) used a quasi-steady method to investigate the random suspension of particles at finite Reynolds numbers. By using a finite-element model, Feng and Joseph (1995) showed that inertia might change the behavior of the particle motion even in creeping flow when the particle size is comparable to that of the width of the settling chamber. Koch and Hill (2001) also pointed out that particle inertia plays a very important role in the sedimentation problem. They found out that particle inertia allows the particles to be thrown out of vortices and to accumulate in regions where the vorticity is lower. This is one of the mecha-

nisms on how particle clusters are formed and sustained. Joseph and his co-workers created an algorithm for the direct simulation of particle interactions, based on a finite-element method. They studied the two-dimensional motion of settling particles under gravity at Reynolds numbers up to 600 (Hu et al., 1992; Feng et al., 1994). Later, Hu (1996) used the same method to simulate the motion of 400 particles in Poiseuille flow. Johnson and Tezduyar (1997) used a space-time finite-element method to investigate the sedimentation of 100 spheres in a tube at Reynolds numbers up to 100.

While Frisch et al. (1986) are considered the pioneers in the application of the LBM in fluid flow problems, Ladd (1994a,b) was the first to apply this method to particulate flows and to derive meaningful results from it. Later, Aidun et al. (1998) applied this theory to free-falling particles and incorporated several modifications to it. An excellent review of this computational method, including its use in particulate flows, may be found in a recent article authored by Chen and Doolen (1998). Feng and Michaelides (2002a) also used the LBM to determine the total hydrodynamic force (drag and lift) on a particle attached to a solid boundary, when other particles are suspended in its vicinity. Also, Feng and Michaelides (2002b) used the same method to study the three-dimensional problem of a sphere settling in a viscous fluid that is contained in cylindrical and prismatic enclosures.

Most of the studies on suspension flows deal with particles that are initially randomly distributed in their container. Very few studies exist on how an initially ordered group of particles behaves during the sedimentation process. Feng et al. (1994) and Qi (1999) investigated the interactions of two particles settling under the gravity in a channel, while Caflisch et al. (1988) and Phillips (1996) considered three or four particles in such a process. Qi (2000, 2001) also simulated the flow of a group of rectangular particles falling in two- and three-dimensional channels and found that the particle behavior is dominated by the wakes, which arise because of the inertia effects.

When a large number of particles is allowed to fall freely under gravity in an otherwise clear fluid, it is desirable to know at least qualitatively how this group of particles will settle, whether there is a general shape followed by the system of particles, the formation of any groups/clusters and how the suspension "expands" as the particles settle. Ensemble-averaged particle velocities, velocity fluctuations and local concentrations are also desirable to be known. In this study we use the LBM to simulate the two-dimensional sedimentation processes of groups of non-cohesive particles. We determine the instantaneous velocities of all the particles and derive the ensemble-average velocities, the instantaneous velocity field of the interstitial fluid and the instantaneous concentrations of particles. We follow the formation of particle clusters and determine the effect of such clusters on the velocities of the individual particles as well as the average velocity of the whole ensemble. Thus, we are able to explain better the origin of the velocity fluctuations and certain other salient features of sedimentation dynamics. Because the problem is computationally intensive, we have used two-dimensional particles for the simulations. Although this may be a drawback of the study, the information obtained from the simulations, such as the formation and breakup of clusters of particles that flow together, the dependence of the average settling velocity on the number and lateral position of the clusters, the effects of particle inertia and the salient features of the sedimentation process are qualitatively applicable to the case of real three-dimensional particles.

2. The Lattice-Boltzmann method

The basic idea behind the LBM is to construct kinetic models that incorporate the essential physics of microscopic processes, so that the macroscopic averaged properties of the model obey the desired macroscopic equations. When the LBM is used to simulate particulate flows, the Lattice-Boltzmann equations should first match the macroscopic Navier–Stokes equations and conform to the desired boundary conditions at the interface of the fluid and particles. Ladd (1994a,b) was the first to use the LBM to simulate particulate flows and developed boundary rules for the fluid and the particles. His work on particulate flow simulations was followed by the studies of Aidun et al. (1998), Aidun and Lu (1995), and Qi (1999). The LBM has several very obvious advantages: It is very simple to be implemented by any programming language, is not difficult to upgrade from two-dimensional to three-dimensional (Feng and Michaelides, 2002b), and can easily treat different shape of particles, such as ellipses and squares as well as different geometries of the fluid containers or flow channels. The LBM is normally used with fixed, regular computational grids, the lattice. Therefore it is not to regenerate the computational grid at each time step in order to account for the motion of particles or boundaries. It also appears that the LBM is especially suitable for computations on particle–fluid interactions since the calculation time only linearly depends on the number of particles.

The LBM is constructed as a simplified, fictitious molecular dynamic in which space, time and fluid–particle velocities are all discrete. The primitive variables in LBM are the fluid–particle distribution functions. The discrete kinetic equation for the distribution function at any point (node) is defined by Chen and Doolen (1998) as

$$f_i(\vec{x}+\vec{e}_i, t+1) = f_i(\vec{x}, t) - \frac{f_i(\vec{x}, t) - f_i^{\mathrm{eq}}(\vec{x}, t)}{\tau}, \tag{1}$$

where f_i is the fluid–particle distribution function, f_i^{eq} is the equilibrium distribution function, τ is the relaxation time and t is the lattice simulation time. The subscript i represents nine symmetric directions in two-dimensions, towards which the particle may move. The coordinates of the nearest neighbor points around $\vec{x}$ are $\vec{x}+\vec{e}_i$. A lattice point may move in the eight directions to its nearest neighboring points, while the ninth direction is the zero vector, signifying that the lattice point is at rest.

At each lattice node/point, the fluid density and momentum are defined based on the distribution function, f_i as follows:

$$\rho = \sum_i f_i(\vec{x}, t), \tag{2}$$

and

$$\rho\vec{u} = \sum_i f_i(\vec{x}, t)\vec{e}_i, \tag{3}$$

where $i = 0, 1, \ldots, 8$. The equilibrium distribution function f_i^{eq} is defined as follows by Chen and Doolen (1998):

$$f_i^{\mathrm{eq}}(\vec{x}, t) = \rho w_i \left[1 + 3\vec{e}_i \cdot \vec{u} + \frac{9}{2}(\vec{e}_i \cdot \vec{u})^2 - \frac{3}{2}u^2\right]. \tag{4}$$

In the two-dimensional space, $w_0 = 4/9$, $w_1 = w_3 = w_5 = w_7 = 1/9$, and $w_2 = w_4 = w_6 = w_8 = 1/36$. To fully recover the Navier–Stokes equations for a viscous fluid, the relaxation time τ is related to the fluid kinetic viscosity v as follows:

$$v = (2\tau - 1)/6. \tag{5}$$

Since there is mass and momentum exchange across the solid boundary, the distribution functions that cut boundary nodes should be properly calculated. For this part of the model, we followed Ladd's (1994a) approach that defines the "bounce-back" collision rule as follows:

$$f_{i'}(\vec{x}, t+1) = f_i(\vec{x}, t_+) - 6w_i(\vec{e}_i \cdot \vec{u}_b), \tag{6}$$

where $\vec{x}$ is the position of the node adjacent to the solid surface, which is moving with velocity $\vec{u}_b$; t_+ is the post-collision time as defined in Ladd (1994a); i' represents the bounce-back link; the direction i is the opposite direction to that of i' and intersects the solid surface. The last term in Eq. (7), $-6w_i(\vec{e}_i \cdot \vec{u}_b)$, accounts for the momentum transfer between the fluid and the solid surface. The flow restrictions imposed by this "bounce-back" rule are sufficient to satisfy the no-slip boundary condition between the fluid and any solid surface. The velocity at the boundary of the particle, $\vec{u}_b$, which matches the fluid velocity, is defined as

$$\vec{u}_b = \vec{V} + \vec{\Omega} \times (\vec{x} - \vec{R}), \tag{7}$$

where $\vec{V}$ is the velocity of the center of mass of a solid particle, $\vec{\Omega}$ is the particle rotational velocity and $\vec{R}$ is the position of the particle center.

The hydrodynamic force exerted on the solid particle at any boundary node can be obtained from the following expression:

$$\vec{F}\left(\vec{x} + \frac{1}{2}\vec{e}_i, t\right) = 2\vec{e}_i\left[f_i(\vec{x}, t_+) - 6w_i(\vec{u}_b \cdot \vec{e}_i)\right]. \tag{8}$$

The total force $\vec{F}_T$ and the torque $\vec{T}_T$ on the solid particles are

$$\vec{F}_T(t) = \sum_i \vec{F}\left(\vec{x} + \frac{1}{2}\vec{e}_i, t\right), \tag{9}$$

and

$$\vec{T}_T(t) = \sum_i \left(\vec{x} + \frac{1}{2}\vec{e}_i\right) \times \vec{F}\left(\vec{x} + \frac{1}{2}\vec{e}_i, t\right). \tag{10}$$

Given the net force and toque, finally the translation and the rotation of the particle is updated numerically as

$$\vec{V}(t+1) - \vec{V}(t-1) = 2M^{-1}\vec{F}_T(t), \tag{11}$$

and

$$\vec{\Omega}(t+1) - \vec{\Omega}(t-1) = 2\vec{I}^{-1} \cdot \vec{T}_T(t). \tag{12}$$

where M is the (scalar) mass of the particle and $\vec{I}$ is the inertia tensor of the particle. In our numerical scheme, we updated the particle displacement by an Eulerian method:

$$\vec{X}(t) = \vec{X}(t-1) + \vec{V}(t-1) \cdot \mathrm{d}t, \tag{13}$$

with the time step dt being one lattice time unit for all the calculations.

Regarding the collisions of the particles, Pan et al. (2002) proposed a method for creating an artificial repulsion force between two touching particles that includes a component along the centerline of the particles and another in the transverse direction (friction component). This force is related not only to the distance of the particles but also on their masses. For simplicity, in this work we use a simpler version of the repulsion force model: When two particles are about to overlap, an artificial repulsion force, F_{r}^{R}, is activated. This force is directed along the centerline of the particles and depends linearly on the overlap distance. The force component in the transverse direction is assumed to be equal to zero:

$$F_{\mathrm{r}}^{R} = \varepsilon \cdot \lambda \quad \text{and} \quad F_{\mathrm{t}}^{R} = 0 \tag{14}$$

where ε is a constant, which was taken to be equal to 5 in the simulations and λ is the overlapping distance. Fig. 1 illustrates the use of the repulsion force. While it is important to include a repulsion force in order to avoid overlapping, we have found out from the simulation results that the coefficient ε does not appreciably affect the overall behavior of the ensembles of particles. Thus, we have obtained very similar results on the behavior of the ensemble as well as the formation and breakup of clusters when the parameter ε is in the range 1–10.

Throughout this study, the diameters of circular particles are always kept as 20 lattice units length and the kinetic viscosity v is always 0.1211 in lattice units. This value corresponds to the viscosity of pure water. The time, T, which is reported in our simulation results, was made dimensionless by the characteristic time of the particles, $\tau_{\mathrm{p}} = \rho_{\mathrm{p}} d^2/(18\mu_{\mathrm{f}})$.

Because the group of particles expands in the flow field, adjustable boundaries were used to simulate the sedimentation process. The upstream boundary condition in the computational domain is zero velocity, which signifies a deep channel. This boundary is always at least $10d$ ahead of the first particle. The downstream boundary condition is stress-free and allows the development of a wake. The computational domain is adjusted for this boundary to be at least $15d$ behind the last particle. As the sedimentation process progresses, the particles move with unequal velocities and the computational domain is enlarged in the y direction. Fig. 2 shows the coordinate system and the flow domain of the simulations. This type of computational domain was used by Qi (1999) and Aidun et al. (1998). They found that it yields sufficiently accurate results in particulate flows. Two values for the Reynolds number, based on the properties of the particles, were used in the

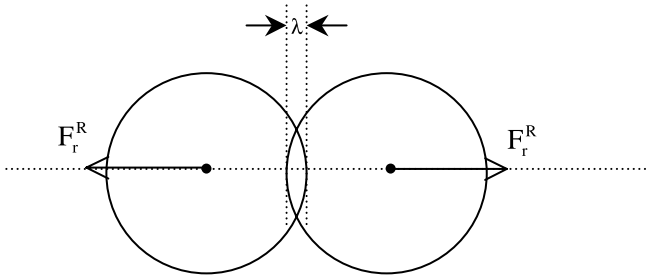

Fig. 1. Illustration of the repulsive force.

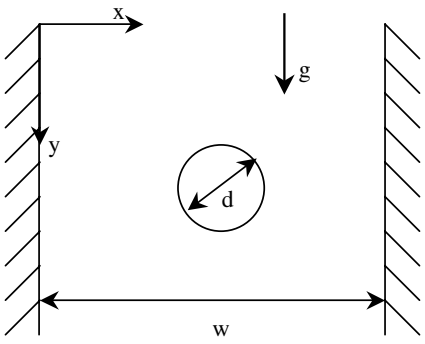

Fig. 2. Coordinate system used in the simulations.

numerical computations: a low Re, of ≈ 0.6, where the inertia effects of the particles are weak and a higher Re, of ≈ 6, where there are strong inertia effects. The computations were carried in a SGI Onyx 3400 machine with eight processors of 400 MHZ R12000. The CPU time for a full simulation with 100 particles is ≈ 22 h. CPU times with a lesser number of particles typically run about 15 h.

3. Simulation of the process of sedimentation and results

3.1. Validation of the method

In order to validate our LBM algorithm, we compared our results with those obtained by Aidun and Lu (1995) who also used the LBM and Feng et al. (1994) who used a finite element scheme. We followed the motion of a disk of diameter d, which is released in a two-dimensional channel of width $4d$ under gravity, with zero initial velocity. The Reynolds number based on the size of the particle is defined as

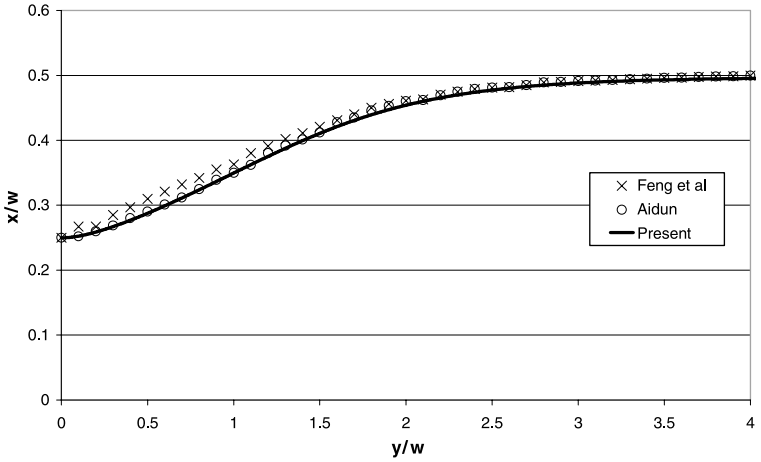

Fig. 3. Single particle trajectories in the narrow channel at $Re = 1.03$.

$$Re = d \cdot V_t / v. \tag{15}$$

The terminal velocity of the particle, V_t can be numerically calculated by releasing a particle in the center of an infinite channel and let it move under gravity until it reaches steady state. Fig. 3 shows the results of the flow simulations by depicting the particle trajectory obtained from the present study as well as the trajectories reported by Feng et al. (1994) and from Aidun and Lu (1995). All these simulations are at $Re = 1.03$. It is evident that there is a good agreement of the results of the three approaches. The slight discrepancy in the three trajectories, and especially in the one by Feng et al. (1994), is probably due to the different particle densities and, perhaps, to the particle size, two parameters that were not reported.

3.2. The effect of inertia

The inertia of particles is very important to their motion at $Re > 1$. Feng et al. (1994) showed how the falling pattern changed for two circular particles when the Reynolds number increased from close to zero to a finite number. At high Reynolds numbers the effects of particle inertia become significant and the two particles move in tandem in a pattern of motion that has been named "drafting, kissing and tumbling (DKT)." This behavior of particle motion was first observed experimentally by Fortes et al. (1987) and then was numerically simulated by Hu et al. (1992), Feng et al. (1994) and Qi (1999).

We investigated the importance of the inertia on the motion of the particles by releasing two circular particles in a vertical channel of width $11d$. The initial positions of the particles are midway between the centerline of the channel and one wall, and the inter-particle distance is $2d$. We depict some of the results of the simulation in Fig. 4, which shows snapshots of the particles' positions for the two values $Re = 0.6$ and 6.2. It is obvious that the hydrodynamic interactions between the particles are very weak when $Re = 0.6$ and that the two particles are not approaching very close to each other. The relative position of these two particles is relatively stable after a

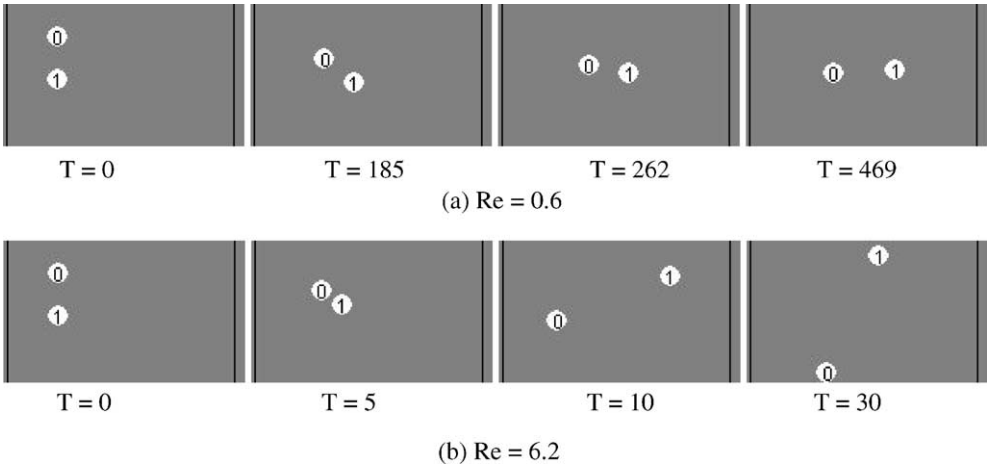

Fig. 4. The DKT pattern of motion of a pair of particles at $Re = 6.2$ and 0.6.

dimensionless time $T = 468$ and the two particles continue their motion parallel to each other. The DKT motion has not been observed in this case. However when $Re = 6.2$, the effects on particles are significant, the relative motion of the particles is very different and the particles come very close to each other on several occasions. The four snapshots in Fig. 4 indicate that the in the interval $0 < T < 30$ the particles move very close and then separate in a pattern of motion that mimics the DTK behavior the others have observed. This pattern repeated itself several times during the simulation of the process.

The results of this simulation show that particle inertia plays an important role in the hydrodynamic interactions between particles. In the computations that follow, the Reynolds numbers based on the terminal velocity of an individual particle are significant enough, between 6 and 7, for the particle inertia to play an important role on the hydrodynamic interactions of the whole ensemble.

3.3. Simulation of the sedimentation of a 7×7-particle array

This part of the study focuses on the sedimentation process of a group of N_P two-dimensional particles, starting from a uniform initial configuration. The density ratio of particles to fluid is equal to 1.00001. During the sedimentation process, the velocities of the particles are unequal and the ensemble expands. As a result, the average concentration of the ensemble, which is defined as

$$\phi = \frac{N_P \pi d^2}{4hw} \tag{16}$$

decreases monotonically during the sedimentation process. We decided to present the results of the simulations with respect to the average concentration and not to any "local" concentration, which depends on a smaller control volume, because any type of calculation of the "local" concentration would involve substantial errors, due to the movement of the particles through the smaller control volume. Fig. 5 shows the way of calculation of the concentration, while Fig. 6 depicts a typical initial configuration that was used for the simulation with a 7×7 array of particles. For the fluid and particle dimensions and properties assumed the Reynolds number

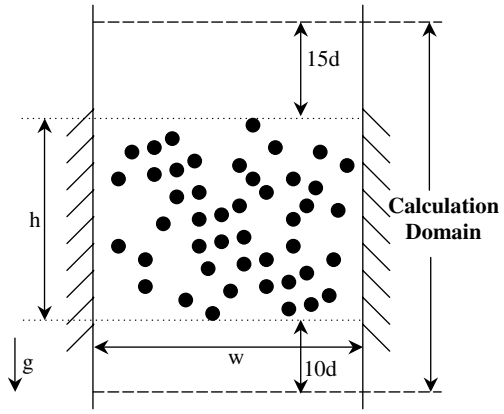

Fig. 5. Illustration of the definition of particle concentration.

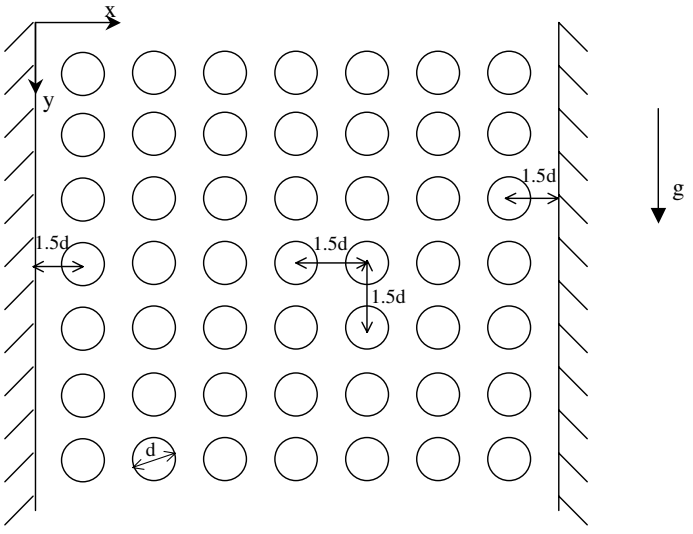

Fig. 6. Initial configuration and coordinates for the 7×7 particle array.

based on the terminal velocity of a single particle is 6.2. At this Reynolds number the viscous effects are not negligible, but particle inertia plays an important role as demonstrated in the previous section.

The particle ensemble average longitudinal and transverse velocities, V_y, and V_x, are shown in Fig. 7 during the sedimentation process. All the velocity values are normalized by the terminal velocity of a single particle, V_t. Due to the particles' symmetric configuration in the initial stages of the computation, the transverse velocity V_x is close to zero in the beginning of the sedimentation process, but does not stay there for a long time. Since the system is highly non-linear and particle interactions are common, fluctuations of V_x occur, the initial symmetric configuration breaks down and particles move in all directions. As a result, particles move horizontally, influenced by interactions with the walls and with other particles. The velocity component, V_x, fluctuates around zero, but is finite with the maximum magnitude of the fluctuation being about 10%. The other component of the particle velocity, the longitudinal component, V_y, increases monotonically and reaches a value close to the terminal velocity, V_t. The value of V_y appears to reach a steady value and to fluctuate around a value that is a little higher than the terminal velocity, $1.1V_t$. Throughout the simulation it was clearly observed that the maximum value of the longitudinal velocity, V_y remains between $1V_t$ and $1.2V_t$. The ensemble-average velocity is higher than the terminal velocity because of the formation of clusters that move faster than individual particles.

During the sedimentation process hydrodynamic forces develop between the particles themselves and between the particles and the vertical walls of the container. The tighter a group of particles is, the stronger the interaction forces would be. As a result of the hydrodynamic interactions we observe the formation and breaking of particle clusters, the influence of wakes on individual particles and a rather weak repulsion of the walls on the particles. In order to describe the process of the particle settling, one may define a particle dispersion function in both the horizontal and the vertical direction as follows:

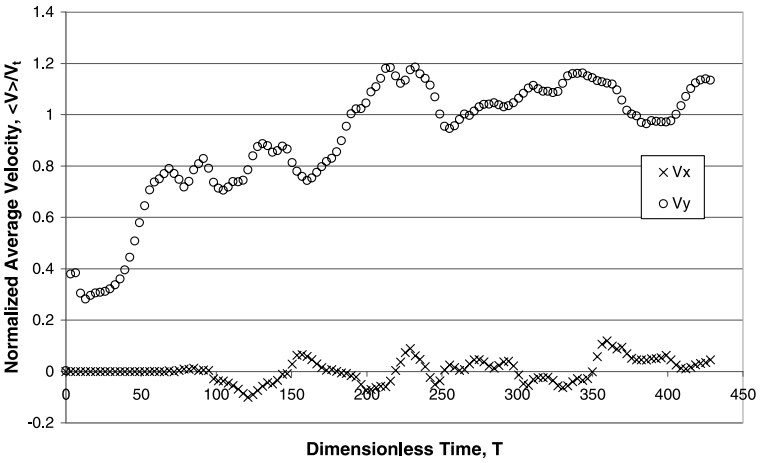

Fig. 7. Average velocities for the 7×7 particle array.

$$D_i = \frac{1}{N_P}\left(\sum_{k=1}^{N_P}((X_i)_k - \langle X_i\rangle)^2\right)^{1/2} \tag{17}$$

where subscript i indicates either x for the horizontal direction or y for the vertical direction. $\langle X_i\rangle$ is the average displacement in the ith direction. All the averages in this study are ensemble averages.

Fig. 8 shows the dispersion changes for the 7×7 uniform array. The particles initially are evenly located in the transverse direction. Because of the particle–wall interactions, the group of particles cannot expand horizontally and, therefore, the dispersion in x fluctuates weakly around its initial value. It is important, however, to note that there are fluctuations in D_x, which indicate that there are dynamic interactions of the particles that affect significantly their transverse motion. On the other hand it is observed that the dispersion in the longitudinal (vertical) direction, D_y, increases almost monotonically. The reason for this is that particles can travel almost without

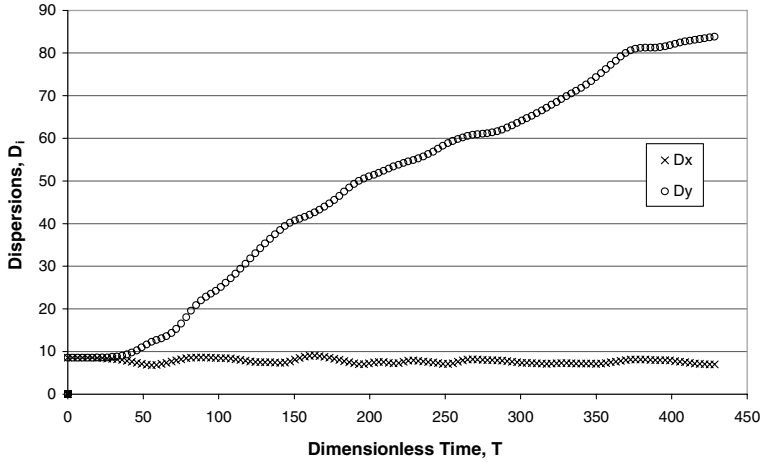

Fig. 8. Dispersions for the 7×7 particle array.

restriction in the vertical direction. The particles in the front move in general faster, while the particles on the back move slower. The formation of particle clusters facilitates their motion, since the clusters would move as a bigger particle, which has higher terminal velocity. It was observed from videos of the motion that, during this process of sedimentation, several clusters (mainly two or three particles) were formed for a short duration and then split apart. This phenomenon of cluster formation is quite different from the DKT pattern of settling of only two particles, which was described by Feng et al. (1994). On a few occasions we have seen the DKT behavior between pairs of particles, but not very often. The cluster formation and break-up of more than two particles was the predominant mode of interactions after the system of particles overcame the constraints of its initial configuration. In most cases, we observed effects of third or fourth particles joining a pair, separation of two particles that join different pairs in the settling process, wall interactions, as well as the temporary formation of many-particle clusters. These clusters produce large wakes and exert very strong influence on the surrounding particles. As a result of these complex interactions, in the 7×7 particles sedimentation process, we did not observe any periodic characteristics.

One of the objectives of this study is to determine the relationship between the average settling velocity of the groups of particles and the volumetric concentration. During the simulation of the sedimentation process of the 49 particles, the concentration of the mixture decreased from the initial value of 35% to values of the order of 5%. Fig. 9 depicts the results for the average terminal velocity of the ensemble of particles, versus the instantaneous concentration of the particles. It is apparent from this figure that an exponential function for the dependence of the terminal velocity on the concentration, such as the Richardson and Zaki (1954), expression would fit the simulation results fairly well. It must be pointed out that the left-most side of the curve corresponds to the stages towards the end of the simulation, when the concentration is low. It is shown that, in this range, the ensemble-average terminal velocity oftentimes exceeds the terminal velocity at vanishing concentration and attains a value closer to $1.1V_t$. We believe that this is due to the formation of several clusters of particles, which move faster than a single particle.

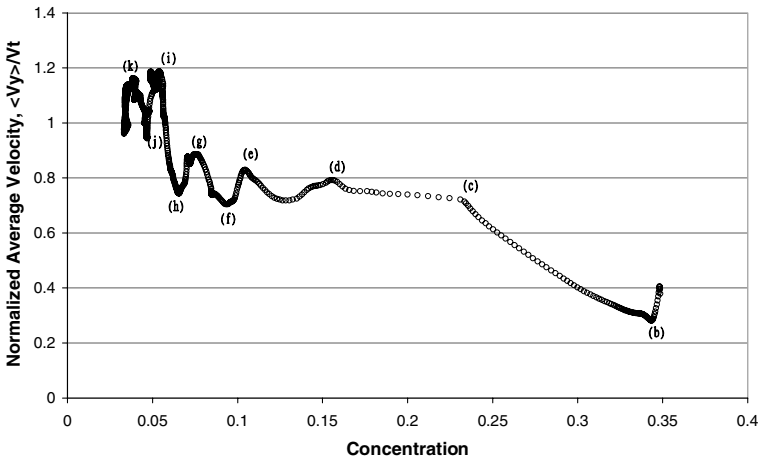

Fig. 9. Average settling velocity of particles as a function of the instantaneous concentration.

This assertion is elucidated in Fig. 10, which shows several instantaneous positions, (a) to (k) of the ensemble of particles with the instantaneous concentration, ϕ. The states of the ensembles (b) to (k) are also indicated in Fig. 9. All the particles in the velocity field are identified by a number, from 0 to 48. The initial symmetric position of the ensemble of particles is shown in part (a). At this stage, the concentration of the ensemble is at the highest value, ≈ 0.35. Shortly after the commencement of the process, at $T = 16$, the array of particles maintains its initial order and the concentration decreases to $\phi = 0.34$. There are no visible clusters formed at this stage. At this stage it is noticed that the groups of particles that initially formed the rows of the matrix of the ensemble are actually deforming to V-shaped formations, which remain visible up to $T = 57$. This is due to the fact that the particles close to the center would move faster, while the particles closer to the walls would be retarded by their interactions with the walls. With the V-shaped front, the whole ensemble experiences less drag and moves relatively faster. The V-shaped formations are still evident in Fig. 10(c) with the bottom row having a very sharp V-shape and the upper row having an identifiable, but flatter V-shape. It is of interest to note that at this stage the columns close to the two walls have formed arches that "compress" the ensemble in the transverse direction.

At stage (c) the formation of the first clusters is obvious, such as cluster 35-42-43 and cluster 31-38-45. These clusters of particles remain together as can be seen in the next two figures, 10(d) and 10(e) and their flow starts playing an important role in the sedimentation process. The V-shaped rows, which are a product of the initial configuration of the array, are still identifiable in stage (d), but not at stage (e). At this stage, the formation and break-up of clusters dominates the sedimentation process. It must also be noted that the inwards facing arches close to the walls at stage (c) have been changed to outwards facing arches, thus resulting in an "expansion" effect. Both the compression and the expansion effects in stages (c) and (d) can be identified in the transverse dispersion curve of Fig. 8 as the trough and peak at $T = 57$ and 69.

A glance in the subsequent parts of Fig. 10 shows that, from this stage onwards the original symmetry of the configuration that gave rise to the V-shaped shear layers has been destroyed, and that the formation and break-up of clusters is the main mechanism that controls the sedimentation velocity. The clusters affect the whole system of particles in two ways: First, a cluster of particles settles faster than a single particle, because of its size. Second, the wake generated by a cluster is much stronger than that from a single particle and, hence, the wake region influences more the rest of the particles. Stages (e), (f) and (g) show the influence of the clusters and wakes on the motion of the rest of the particles in the ensemble. We have used the same coordinates in these three figures in order to show in more detail the motion of individual particles. Also, the fluid velocity vectors at these three stages are depicted separately in Fig. 11 in order to show the influence of the clusters of particles on the fluid velocity field.

A typical example of cluster–particle interaction that merits attention is that of particle 24 with the cluster of particles 31-38-45: It is obvious through stages (e), (f) and (g) that particle 24 falls in the wake of the cluster of particles 31-38-45 and is accelerated by this wake. The final result of the interaction for particle 24 is to join particles 38-45 in the formation of a new cluster, while at the same time expelling particle 31 from this cluster. It is also observed from Fig. 9 that the average velocity at stage (f) is below the trend, while the average velocity in (e) and (g) is above this trend. This is due to the formation and flow of the clusters as well as to particle–wall interactions. Even though stage (f) does have a few clusters, most of them are located at the top and close to the walls

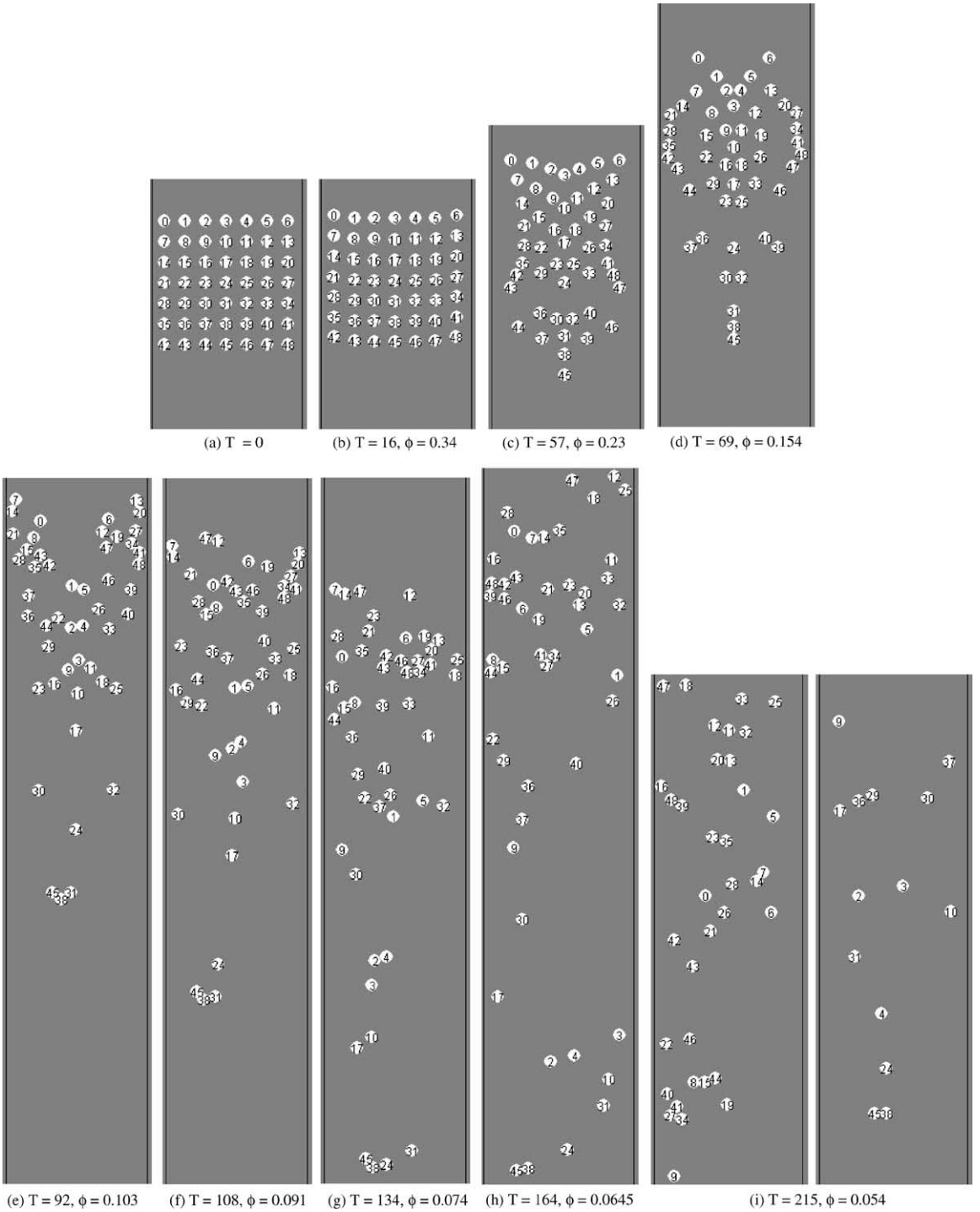

Fig. 10. Instantaneous positions of particles at several stages of the sedimentation process marked in Fig. 9.

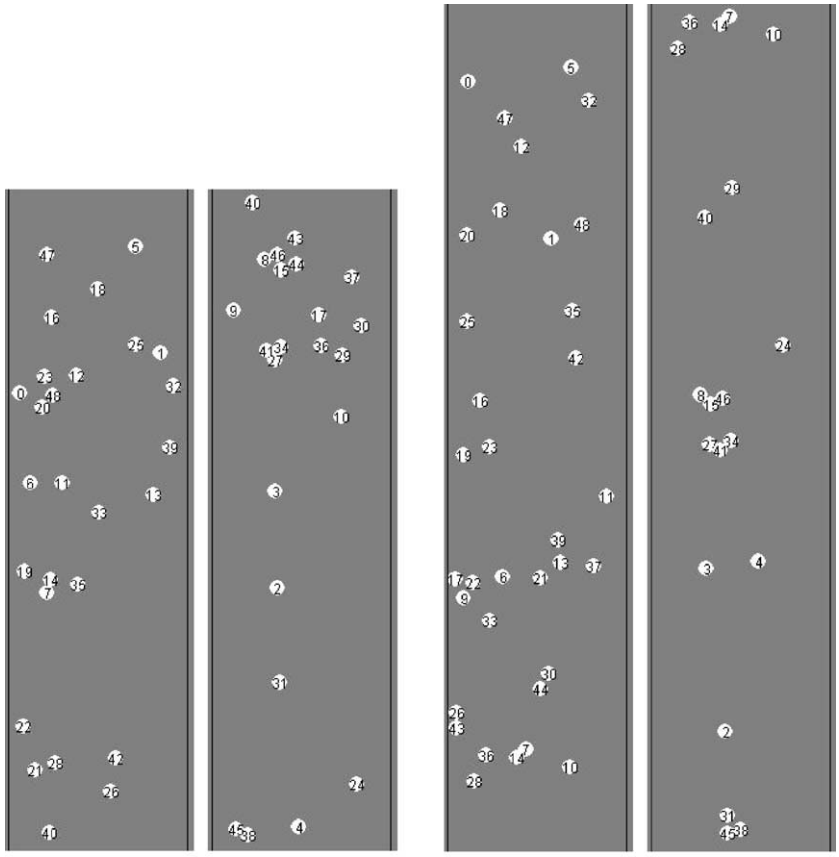

(j) T = 259, ϕ = 0.046 (k) T = 346, ϕ = 0.038

Fig. 10 (*continued*)

of the system, where the motion is slower and where strong vortices sweep some particles upwards. Fig. 11 shows the velocity vectors and corroborates this observation: It is apparent that at stage (e) there is a very strong downward flow channel in the middle of the container and many particles are carried by this flow. At stage (f) there are several particles, such as 23, 16, 29, 22 which are trapped in the upward motion of a vortex. This results in slower overall sedimentation velocity for the whole ensemble. At stage (g) all of the last particles, except 16, have migrated towards the center, where the fluid velocity field has a strong downwards component. One of the characteristics of the sedimentation process at this stage is that many clusters break-up and others are formed. For example, the cluster 3-11-18-25 at stage (e) breaks out and does not exist in stage (f).

It is interesting to note some of the interactions of the particles and clusters. It is observed in stages (d), (e) and (f) that the pair-cluster 42-43 shows the typical ''kiss-and-tumble'' behavior that has been observed in systems of two particles. It is clear that these two particles are in a vorticity field, which circles counter-clockwise in the top-left of the container. This behavior is the result of particles 42 and 43 circling in the vorticity generated by the interaction of other particles. Other

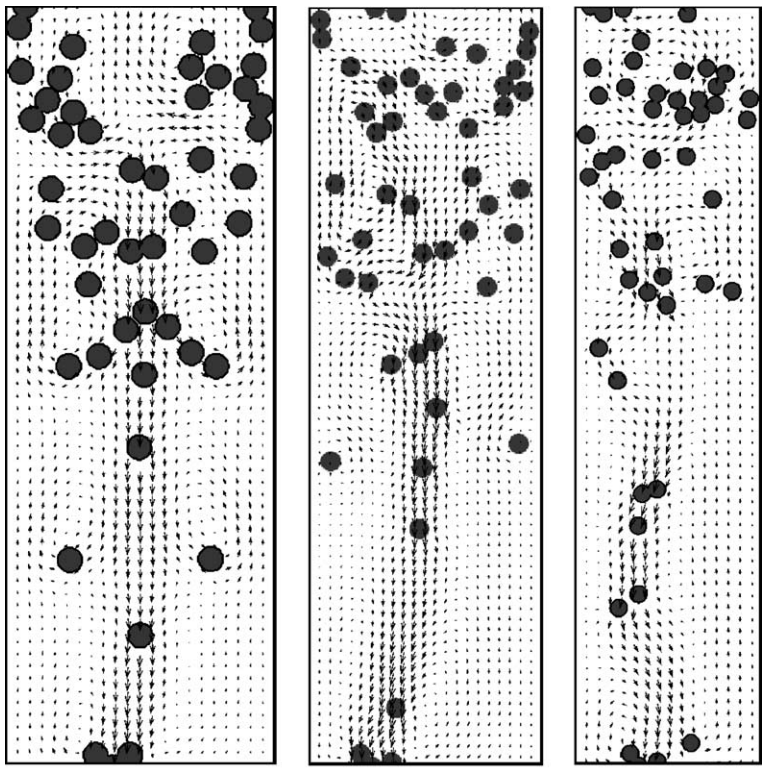

Fig. 11. Instantaneous positions of particles and velocity fields.

clusters follow a more complex behavior. For example, cluster 13-20-27-34-41-48 of stage (e) and stage (f) moves to the middle of the channel at stage (g). Particles 6 and 19 are "trapped" by this big cluster at this moment and will be induced to move faster. At stage (h) it is clear that these two particles have accelerated sufficiently to overtake some other particles, such as particles 32, 33, 42 and 43, while the big cluster has broken. At this stage, particle 6 loses contact with the cluster while particle 19 is still in the wake of the remainder of the cluster, 27-34-41. As a result, at the next stage, (i), particle 19 continues to move faster and almost overtakes the last cluster, while particle 6 lags far behind. Then, particle 19 is shed towards the wall and decelerates. In the meantime the cluster 27-34-41, which stays together and moves towards the center of the channel, overtakes particle 19 and leaves it far behind at stage (j).

Such observations illustrate two points: First, clusters in the center of the channel move faster and generate stronger wakes than single particles or than clusters near the walls. Second, particles in the wake of a cluster will move faster than other particles.

The unsteady wakes generated by clusters and particles not only help particles accelerate, but also push particles backward. Some retrograde motions were observed during the simulations. For example, particles 23 and 25 move backwards between stages (e), (f) and (g) after being pushed outwards and backwards by faster moving clusters.

The fluid velocity fields in Fig. 11 show the following trends: First, there is a central downward flow channel, which is basically created by the leading particles. Particles in this central channel will be accelerated and move faster. Second, the fluid close to the wall is occasionally flowing backward and always has very low velocity. This is why particles in this region mostly move backwards or, if they move forwards, their velocities are very low. Third, there are some distinct vortices in the field, which make the fluid field complicated and make the particles to move to the sides. Vortices may make particles to move forward fast, such as particle 37, 40 in stage (f), or move backward, such as particle 23, 25 in stage (e), or stay almost still, such as particle 11, 32 in stage (f). A glance at all the parts of Figs. 10 and 11 prove that the initially orderly array of particles behaves in a very complex way and that the velocity fluctuations observed in Fig. 9 are mainly due to the formation and break-up of particle clusters, their interaction and their interactions with the walls of the channel.

From the numerical simulations, we define three stages in the sedimentation process:

1. During the first stage, the initial orderly condition of the arrays plays an important role on the process, the average sedimentation velocity and the rate of decrease of the concentration. The "V-shaped" formations are the characteristics of this stage.
2. During the second stage, the sedimentation process is mainly influenced by the flow of clusters and the interactions of clusters and particles with the walls of the channel.
3. During the last stage, the concentration of the ensemble is low enough for the system to be considered dilute, $\phi < 0.06$, and the interactions of particles outside the already formed clusters play a lesser role as shown in stages (i), (j) and (k) of Fig. 10.

The last three stages have been depicted in two columns, because of the expansion of the system. In these stages, the clusters are relatively stable. Very few new clusters are generated, and very few existing clusters break down. The reason the average velocity in (j) is lower than that of (i) and (k) is that leading cluster 38-45 has moved close to the wall and its wake does not assist the trailing particles to move faster. When this leading cluster is back in the center of the channel, as in stage (k), the ensemble average velocity reaches a higher value.

3.4. Velocity fluctuations and particle distribution

The particle velocity fluctuations reflect the intensity of the particle interactions during the sedimentation process. We calculated the particle velocity fluctuation defined as

$$V_k^{\mathrm{fl}} = \frac{1}{N_{\mathrm{P}}} \sum_{i}^{N_{\mathrm{P}}} \frac{((V_k)_i - \langle V_k \rangle)^2}{\langle V_k \rangle^2}, \tag{18}$$

where V_k represents the velocity of the kth particle. Figs. 12 and 13 depict the fluctuations for the vertical velocity, V_y, and the total velocity, $V_{\mathrm{total}} = \sqrt{V_x^2 + V_y^2}$, of the particles in a 7×7 array when $Re = 0.6$ and 6.2. It is observed in both figures that the intensity of the vertical velocity fluctuations is higher than the intensity of the total velocity. This occurs because the horizontal velocity, V_x, which is a component of the total velocity, is restricted in its fluctuations by the container walls and, in addition has a lower magnitude than the vertical velocity component.

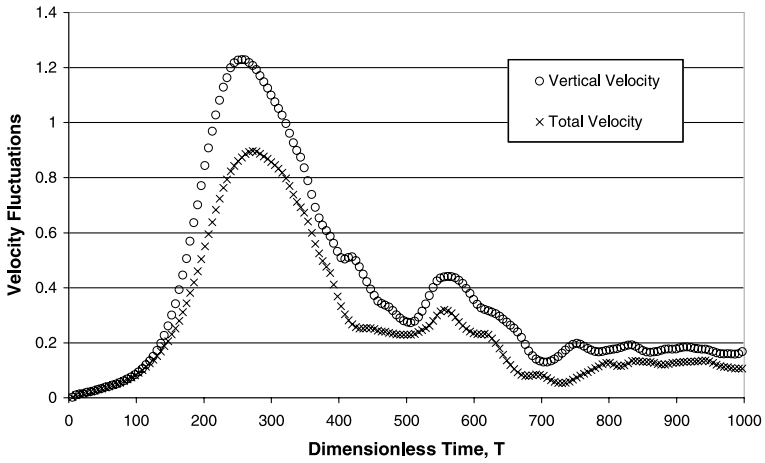

Fig. 12. Velocity fluctuations for a 7×7 particle array at $Re = 0.6$.

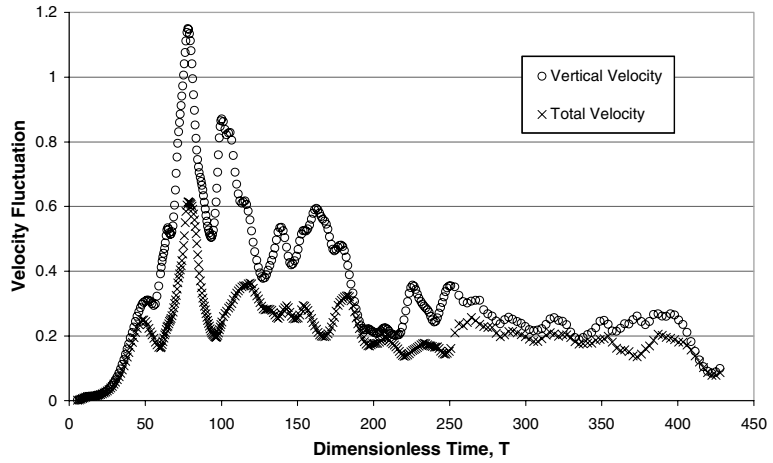

Fig. 13. Velocity fluctuations for a 7×7 particle array at $Re = 6.2$.

It is observed that the first peak of the fluctuations corresponds to the formation of the V-shape in stage 1. In this stage, the particles at the center of the channel start moving faster than those closer to the walls. It is observed that, at $Re = 0.6$, the velocity fluctuations decrease fast after $T = 550$, when the V-shape front breaks and that particle interactions occur less frequently. However, at $Re = 6.2$, it is evident that velocity fluctuations are still strong in the second stage, which lasts approximately up to $T = 250$. During this stage, the particle interactions are strong and particle clusters form and break frequently, thus contributing significantly to the velocity fluctuations. At $Re = 6.2$, during the third stage, from $T = 250$ onwards, the velocity fluctuations weaken. In this stage the system is dilute ($\phi < 0.05$) and the particle clusters are relatively stable.

Oftentimes during sedimentation processes particle channeling is observed close to the center and the particles move closer to the center. In order to obtain a measure of the channeling we

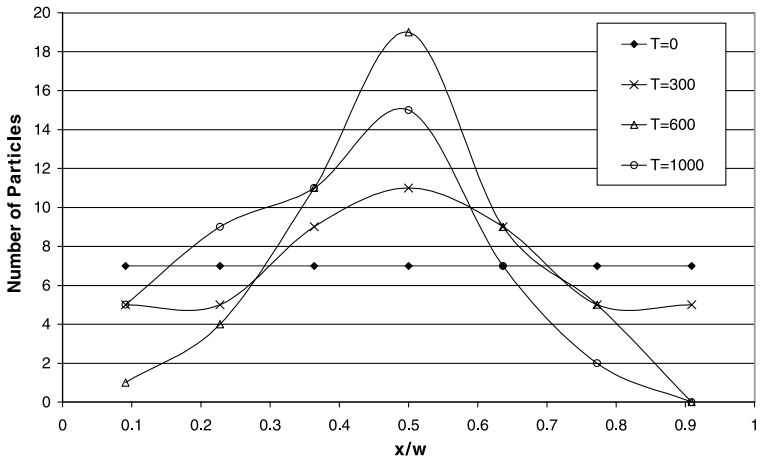

Fig. 14. Particle distribution in the x direction for a 7×7 particle array at $Re = 0.6$.

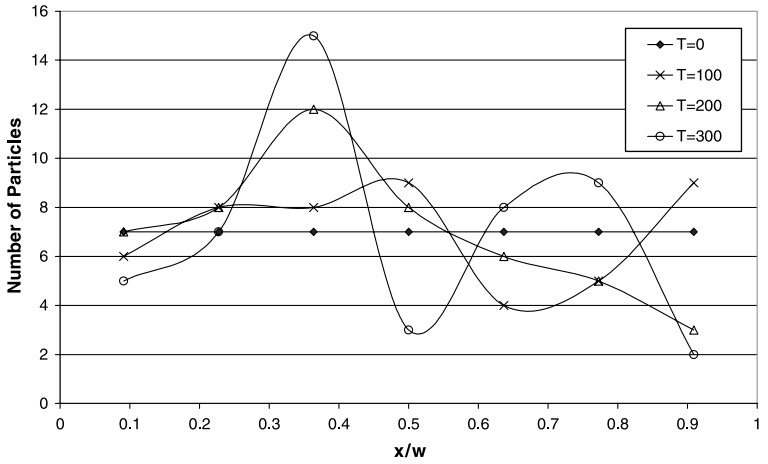

Fig. 15. Particle distribution in the x direction for a 7×7 particle array at $Re = 6.2$.

calculated the particle distribution across the channel. The results of the 7×7 array are shown in Figs. 14 and 15 for $Re = 0.6$ and 6.2 respectively. In both cases the particle distributions commence with a uniform profile, which is then transformed into a symmetric curve when the V-shape formation occurs. Subsequently, at the higher Reynolds number, $Re = 6.2$, particles move more randomly, interact in a stronger way, their velocities fluctuate more violently and their transverse distribution becomes asymmetric. On the contrary, the distribution of the system of particles with lower inertia ($Re = 0.6$) is almost always symmetric, while more particles tend to concentrate towards the center of the channel. This is due to the relative stability of the clusters formed with the relative tranquility of the flow, as corroborated by the fluctuations results and the qualitative results on interactions described in the previous subsections.

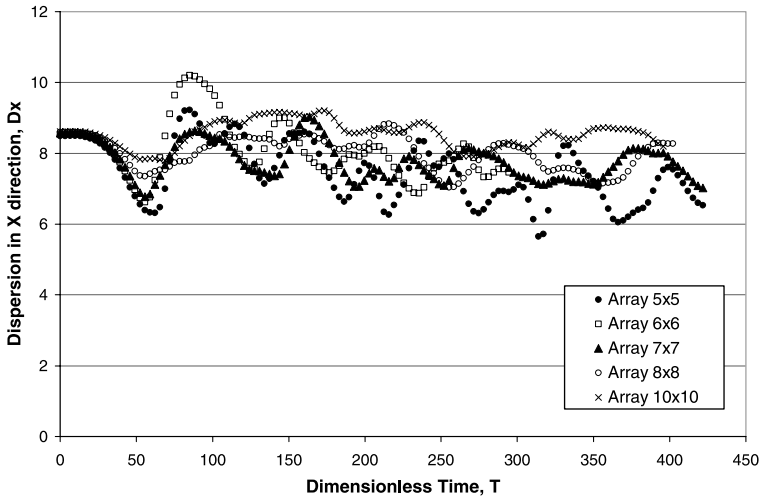

Fig. 16. Dispersions in the x direction for the five array configurations.

3.5. Simulations of particle sedimentation in other initial configurations

In order to study more thoroughly the sedimentation process of a group of particles, we also conducted investigations with initially square arrays of 5×5, 6×6, 8×8 and 10×10 particles and the same inter-particle distance $1.5d$. Since the widths of the walls are different in each case, the Reynolds numbers for a single particle settling along the centerline are 5.71, 6.01, 6.35 and 6.53 respectively. For each array we observed the evolution of the particle dispersion. Fig. 16 shows the changes in the transverse dispersion, D_x, for the five configurations examined. It appears that the instantaneous value of D_x, which is equal to 8.3 at the inception of the process, drops slightly and fluctuates around a constant value of 7.2. The range of variation is from 6 to 10. There seems to be no relationship between the magnitude of the fluctuation and the amount of particles in the ensemble.

Fig. 17 depicts the longitudinal dispersions, D_y, of all the ensembles. It is of interest to note that the dispersions of the ensembles with an odd number of particles, such as arrays 5×5 and 7×7, are almost the same and that they increase faster than the dispersions of the ensembles of even number of particles, such as arrays 6×6, 8×8 and 10×10. The dispersions of the latter arrays increase at almost at the same rate as well. The reason for this observation is that, in the odd-numbered arrays, there is a single central column, whose particles move faster than those of the other columns in the longitudinal direction, because the transverse forces from the left side balance those from the right side. As can be seen in Fig. 10, at stage (d), particles that have started the process in a horizontal row have formed V-shaped layers that move faster. Thus, the particles 45, 38 and 31 which were initially at the central column move down faster, take the lead and form a cluster that leads the pack. The same particles are always in the lead and form clusters of two or three particles in the remaining stages. The wake created by this leading cluster is strong and induces the other particles downstream to move faster.

On the contrary, for the even-numbered particle configurations, there is not a central column, but two. Particles in these two columns experience transverse forces that tend to move both

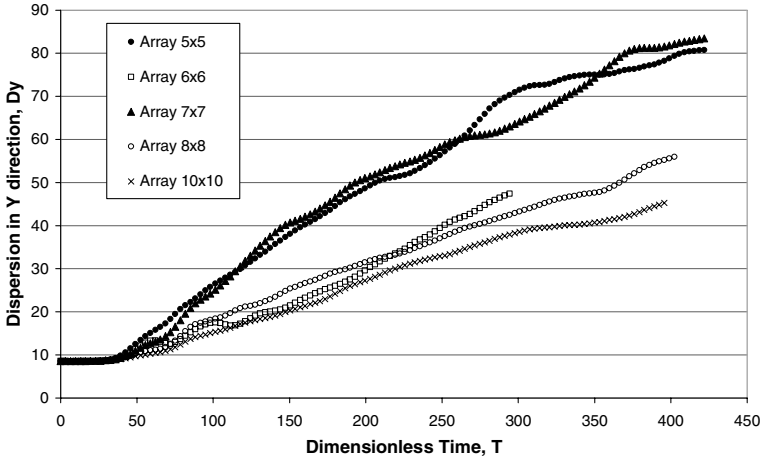

Fig. 17. Dispersions in the y direction for the five array configurations.

columns towards the center, thus competing among themselves for the positions in the center channel. Therefore, the V-shaped layers are not formed and there is not a definite cluster of particles that takes the lead. This is depicted in Fig. 18, which shows one of the initial stages for

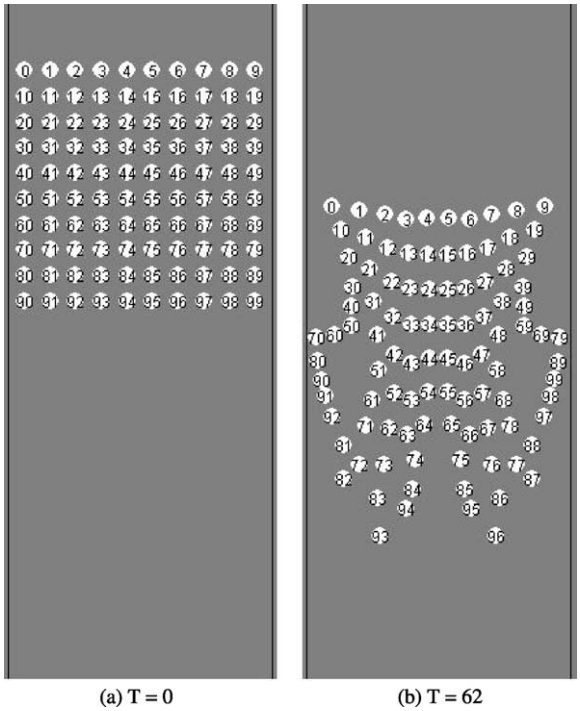

Fig. 18. Instantaneous positions of particles during the initial stages of the sedimentation process for the 10×10 array.

the sedimentation process of the 10×10 array. It is evident in this figure that the bottom row of particles has been deformed into a W rather than a single V formation. As a result, there is higher drag during the initial stages of the process and this results in lower longitudinal velocities and, hence, lower rate of increase of the longitudinal dispersion, D_y.

4. Conclusions

We have employed the LBM to investigate the particle sedimentation in a two-dimensional channel with initially homogeneous square configurations. Specifically, we have tried to clarify two characteristics of the sedimentation process, the dispersion of the particles and the relationship between the ensemble-average sedimentation velocity and the instantaneous concentration of the ensemble. Since the vertical walls contain the ensemble of particles, the fluctuations of the transverse dispersion are very low. The dispersion in the longitudinal (vertical) direction increases almost linearly with respect to time. We have observed that the rate of increase of the longitudinal dispersion depends strongly on whether or not there are one or two central columns of particles. The formation of the V-shaped fronts in the initial stages of the sedimentation process, which is the characteristics of the arrays with one central column of particles, is the main reason for the faster separation of the front from the back rows and of the higher rate of increase of the dispersion.

We have also observed that the sedimentation processes of a homogeneous array of particles may be divided in three stages: During the initial stage when the concentration is high, the initial configuration plays an important role. A particle front is formed during this stage, which may be V-shaped or W-shaped. V-shaped fronts move faster and result in higher rates of increase for the longitudinal dispersion. The second stage is dominated by the hydrodynamic interactions of the particles. Cluster formation and breakup occurs and the motion of clusters plays a key role in the sedimentation process. Because clusters move faster than individual particles, the presence of many clusters leads to higher ensemble-average velocity of sedimentation, while the presence of only a few clusters has the opposite effect. The arbitrary formation and breakup of clusters is also the cause of the wide fluctuations of the ensemble-average velocity. During the second stage, wakes created by the clusters are strong and induce individual particles to move faster or even to drift upward. During the third stage, the values of the concentration are low, particle interactions are weaker and new cluster formations are not as frequent. Existing clusters are very stable and endure the smaller hydrodynamic interactions for a longer time. The velocity fluctuations in this stage are mainly due to the wakes generated by the clusters, especially to the wake of the leading cluster.

Acknowledgements

This work was partially supported by two grants from the Office of Naval Research and USGS to the Tulane-Xavier Center for Bioenvironmental Research (CBR), for which the authors are thankful.

References

Agrawal, K., Loezos, P., Syamlal, M., Sundaresan, S., 2001. The role of meso-scale structures in rapid gas solid flows. J. Fluid Mech. 445, 151–185.

Aidun, C.K., Lu, Y., 1995. Lattice Boltzmann simulation of solid particles suspended in fluid. J. Statist. Phys. 81, 49–61.

Aidun, C.K., Lu, Y., Ding, E.-J., 1998. Direct analysis of particulate suspensions with inertia using the discrete Boltzmann equation. J. Fluid Mech. 373, 287–311.

Batchelor, G.K., 1972. Sedimentation in a dilute dispersion of spheres. J. Fluid Mech. 52, 245–268.

Brady, J.F., Bossis, G., 1985. The rheology of concentrated suspension of spheres in simple shear flow by numerical simulation. J. Fluid Mech. 155, 105–129.

Bunner, B., Tryggvason, G., 2002. Dynamics of homogeneous bubbly flows. Part 2. Velocity fluctuations. J. Fluid Mech. 466, 53–84.

Caflisch, R.E., Luke, J.H.C., 1985. Variance in the sedimentation speed of a suspension. Phys. Fluids 28, 259.

Caflisch, R.E., Lim, C., Luke, J.H.C., Sangani, A.S., 1988. Periodic solutions for three sedimenting spheres. Phys. Fluids 31, 3175–3179.

Chen, S., Doolen, G.D., 1998. Lattice Boltzmann method for fluid flows. Ann. Rev. Fluid Mech. 30, 329–364.

Climent, E., Maxey, M.R., 2001. Numerical simulation of random suspensions at finite Reynolds numbers. Fourth International Multiphase Flow Conference, New Orleans, USA.

Davis, R.H., Acrivos, A., 1985. Sedimentation of non-colloidial particles at low Reynolds numbers. Ann. Rev. Fluid Mech. 17, 91–118.

DiFelice, R., 1999. The sedimentation velocity of dilute suspensions of nearly monosized spheres. Int. J. Multiphase Flow 25, 559–574.

Feng, J., Joseph, D.D., 1995. The unsteady motion of solid bodies in creeping flows. J. Fluid Mech. 303, 83–102.

Feng, Z., Michaelides, E.E., 2002a. Interparticle forces and lift on a particle attached to a solid boundary in suspension flow. Phys. Fluids 14, 49–60.

Feng, Z., Michaelides, E.E., 2002b. Hydrodynamic force on spheres in cylindrical and prismatic enclosures. Int. J. Multiphase Flow 28, 479–496.

Feng, J., Hu, H.H., Joseph, D.D., 1994. Direct simulation of initial value problems for the motion of solid bodies in a Newtonian fluid. Part 1. Sedimentation. J. Fluid Mech. 261, 95–134.

Fortes, A.F., Joseph, D.D., Lundgren, T.S., 1987. Nonlinear mechanics of fluidization of beds of spherical particles. J. Fluid Mech. 177, 467.

Frisch, U., Hasslacher, B., Pomeau, Y., 1986. Lattice-gas automata for the Navier–Stokes equations. Phys. Rev. Lett. 56, 1505–1508.

Hu, H.H., 1996. Direct simulation of flows of solid–liquid mixtures. Int. J. Multiphase Flow 22, 335–352.

Hu, H.H., Joseph, D.D., Crochet, M.J., 1992. Direct simulation of fluid particle motions. Theor. Comput. Fluid Dyn. 3, 285–306.

Johnson, A.A., Tezduyar, T.E., 1997. 3D simulation of fluid–particle interactions with the number of particles reaching 100. Comp. Meth. Appl. Mech. Engng. 145, 301–321.

Koch, D.L., Hill, R.J., 2001. Inertial effects in suspension and porous-media flows. Ann. Rev. Fluid Mech. 33, 619–647.

Ladd, A.J.C., 1994a. Numerical simulations of particulate suspensions via a discretized Boltzmann equation. Part 1. Theoretical foundation. J. Fluid Mech. 271, 285–309.

Ladd, A.J.C., 1994b. Numerical simulations of particulate suspensions via a discretized Boltzmann equation. Part 2. Numerical results. J. Fluid Mech. 271, 311–339.

Ladd, A.J.C., 1997. Sedimentation of homogeneous suspensions of non-Brownian spheres. Phys. Fluids 9, 491–499.

Nicolai, H., Guazelli, E., 1995. Effect of the vessel size on the hydrodynamic diffusion of sedimenting spheres. Phys. Fluids 7, 3–5.

Nicolai, H., Herzhaft, B., Hinch, E.J., Oger, L., Guazelli, E., 1995. Particle velocity fluctuations and hydrodynamic self-diffusion of sedimenting non-Brownian spheres. Phys. Fluids 7, 12–23.

Pan, T.-W., Joseph, D.D., Bai, R., Glowinski, R., Sarin, V., 2002. Fluidization of 1204 spheres: simulation and experiment. J. Fluid Mech. 451, 169–191.

Phillips, R.J., 1996. Dynamic simulation of hydrodynamically interacting spheres in a quiescent second-order fluid. J. Fluid Mech. 315, 345–365.

Qi, D., 1999. Lattice-Boltzmann simulations of particles in non-zero-Reynolds-number flows. J. Fluid Mech. 385, 41–62.

Qi, D., 2000. Lattice-Boltzmann simulations of fluidization of rectangular particles. Int. J. Multiphase Flow 26, 421–433.

Qi, D., 2001. Simulation of fluidization of cylindrical multiparticles in a three-dimensional space. Int. J. Multiphase Flow 27, 107–118.

Richardson, J.F., Zaki, W.N., 1954. Sedimentation and fluidization: Part I. Trans. Inst. Chem. Eng. 32, 35–53.

Segrè, P.N., Herbolzheimer, E., Chaikin, P.M., 1997. Long-range correlations in sedimentation. Phys. Rev. Lett. 79, 2574–2577.

Segrè, P.N., Liu, F., Umbanhowar, P., Weitz, D.A., 2001. An effective gravitational temperature for sedimentation. Nature 409, 594–597.

Stokes, G.G., 1845. On the Theories of Internal Friction of the Fluids in Motion. Trans. Cambridge Philos. Soc. 8, 287–319.